2012

Simultaneous Heat and Mass Transfer in a Wetted Heat Exchanger, Part II: Modeling

Jessica Bock
bock6@illinois.edu

Feini Zhang

Anthony M. Jacobi

Hailing Wu

Simultaneous heat and mass transfer in a wetted heat exchanger, part II: modeling

Jessica BOCK[1]*, Feini ZHANG[1], Anthony M. JACOBI[1], & Hailing WU[2]

[1]University of Illinois at Urbana-Champaign,
Urbana, Illinois, USA
bock6@illinois.edu

[2]United Technologies Research Center,
East Hartford, Connecticut, USA
wuhl@utrc.utc.com

* Corresponding Author

ABSTRACT

An analytical model for a condenser with a wetted surface is developed by applying the governing conservations and rate equations and invoking the heat and mass transfer analogy. The heat exchanger is discretized in both the air-flow and refrigerant-flow directions for a cross-flow configuration. Axial conduction along the tube walls is neglected and uniform distribution of water is assumed at the heat exchanger front fin surface. Any water not evaporated in a finite control volume is assumed to flow into the downstream control volume, and the model is applicable for dry, partially wet, or fully wet surface conditions. Mass and energy balances are applied to each discretized volume (node) to examine the local heat and mass transfer. The model is capable of predicting local heat/mass transfer, wetness condition as well as pressure losses throughout the heat exchanger.

The physics-based model is developed to handle a variety of operating conditions and heat exchanger geometries. Correlations for pressure drop and heat transfer coefficients can be easily replaced or modified for different air-side configurations. The tube-side analysis can also be easily adapted to accommodate different working fluids or tube-side designs. The general framework of the model is robust and flexible.

The model is validated with the experimental data presented in a companion paper, "Simultaneous heat and mass transfer in a wetted heat exchanger, part I: experiments."

1. INTRODUCTION

Evaporative condensers are used in a variety of applications. They can be found in air-conditioning and refrigeration systems to reduce operational power costs. Bare-tube heat exchangers have been predominantly used for evaporative condensers, due to scaling and corrosion issues. Sizing methods are usually simplified by specifying an air flow with 100% relative humidity. Evaporative condensers have also been studied for use in geothermal power plants. Prior work on evaporative cooling in geothermal power plants by Kutsche and Costenaro (2002), Mines (2005) and Ashwood and Bharathan (2011) has clearly demonstrated the performance advantages of using evaporatively cooled condensers in those systems. There have been some investigations of the fundamental heat and mass transfer in heat exchangers with a partially wet air-side surface. However, partitioning the surface into wet and dry areas is difficult and depends on geometry and operation. Most of the work to date has been limited to simple air-side heat exchanger geometries, and to simple water deployment schemes.

In this study, a model is developed for evaporative cooling on a flat-tube, louver-fin heat exchanger. The modeling approach allows for the tracking of wet and dry surface areas. Alternative schemes for deploying the water, either for precooling the upstream airflow or for direct evaporative cooling on the surface of the heat exchanger are explored. The model can be used to predict condenser performance under a variety of conditions, and can be easily manipulated to consider design alternatives.

2. EVAPORATIVE PRECOOLING MODEL

When the ambient air temperature is high, water augmentation can be applied to air-cooled condensers to boost the condenser performance. One method of water augmentation is combined mist precooling and mist deluge cooling. In this approach, mist is generated in the air stream to precool the air, and the remaining mist reaches the condenser surface and cools the condenser. Accordingly, the overall condenser model structure includes the dry condenser model, the wet condenser model, and the air precooling model. If mist precooling is employed, the air precooling model is used to evaluate the conditions at the face of the heat exchanger, which are then applied to the wet model. If deluge cooling occurs, the wet model is used. For no water augmentation, the dry model can be used.

2.1 Droplet Evaporative Precooling Model

Mist evaporative precooling occurs when water is distributed as fine mist via atomizers in the airflow upstream of the condenser. It is followed by mist deluge evaporative cooling at the condenser. Quantifying the response of a population of small droplets to their changing thermal environment is fundamental to understanding the relevant physics. The mass exchange between the droplet and the air controls the evolution of droplet size and changes to the flow. Accurate prediction of droplet evaporation rate and lifetimes is critical to achieving optimal performance of evaporative precooling, especially when water consumption is a constraint. It is also critical to the selection of appropriate droplet generation approaches, such as conventional spray nozzles, air-atomizing spray nozzles or ultrasonic atomizers.

The evaporation characteristics of a single water droplet were examined and compared with data available in the open literature. The water droplet was assumed to be spherical and of uniform temperature. Radiation effects and the relative velocity between droplet and air flows were assumed negligible. A transient energy balance for the droplet can be used to determine the droplet diameter D_d as it changes with time. The energy balance demonstrating the change in the internal energy of the droplet balanced by the convective and latent heat transfer due to evaporation is shown in Equation (1) .

$$\frac{d}{dt}\left(\rho_d C_{p,d} T_d \frac{\pi D_d^3}{6}\right) = \alpha \pi D_d^2 (T_e - T_d) - h_{fg} \dot{m}''_{evap} \pi D_d^2 \tag{1}$$

Adopting the correlation proposed by Whitaker (1972) for flow over a sphere to calculate the Nusselt number, the heat and mass analogy was adopted in the following form to obtain the mass conductance, g_m, following Equations (2-5)

$$Sh_D = Nu_D \left(Sc_e / Pr_e\right)^{1/3} \tag{2}$$

with

$$g_m^* = Sh_D \mathcal{D} \rho_a / D_d \tag{3}$$

$$g_m = g_m^* [\ln(1+\beta_m)/\beta_m] \tag{4}$$

and

$$\beta_m = \frac{y_w - y_{w,s}}{y_{w,s} - 1} \tag{5}$$

Where y_w and $y_{w,s}$ are the mass fraction of water vapor in the air and at the surface of the droplet, respectively.

The evaporative mass flux, $\dot{m}''_{evap}$, is obtained from Equation (6).

$$\dot{m}''_{evap} = g_m^* \beta_m \tag{6}$$

A transient mass balance can be written as Equation (7) to examine droplet lifetime.

$$\frac{d}{dt}\left(\frac{D_d^3 \rho_d}{6}\right) = -\dot{m}''_{evap} D_d^2 \tag{7}$$

A range of operating conditions was applied to the analysis described above to investigate the time variation of the droplet diameter and temperature. The results were compared to experimental data presented by Fujita *et al.* (2010). Overall, the model agreed well with the experimental data and predicted the behavior of an evaporating water droplet.

2.2 Mist Evaporative Precooling Model

A mist evaporative precooling model was developed to predict psychrometric conditions and flow rates of a droplet-laden flow. The water droplets suspended in the air flow can cool the air by evaporation and provide a greater temperature difference upstream of the condenser for enhanced performance. A schematic of the process is shown in Figure 1.

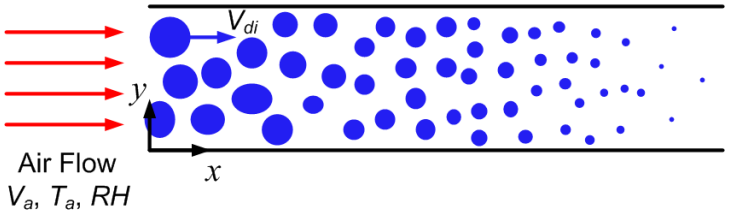

Figure 1: Schematic of the mist evaporative precooling method

The mist evaporative precooling model is based on the conservation of energy. The assumptions from the single droplet approach were applied to a distribution of droplets of uniform velocity and uniform volume, with the moist air and water mist being adiabatically isolated from the surroundings. The volume was calculated for a spherical droplet having a diameter characteristic of the spray method. This diameter was determined experimentally or obtained from atomizer manufacturer.

The rate of droplet production (number of droplets per second) was calculated using Equation (8), for a known water supply rate, $\dot{m}_{spray}$, and initial droplet mass, M_i.

$$N = \dot{m}_{spray} / M_i \tag{8}$$

A mass balance for a droplet gives, with $\dot{m}_{evap} = \dot{m}''_{evap} \pi D_d^2$:

$$N\dot{m}_{evap} = \dot{m}_a \frac{d\omega_e}{dt} \tag{9}$$

Assuming the flow to be adiabatic, conservation of energy for the flowing stream of moist air and droplets gives:

$$\dot{m}_e \frac{dh_e}{dt} + h_e \dot{m}_a \frac{d\omega_e}{dt} + h_d N \frac{dM_d}{dt} + NM_d \frac{dh_d}{dt} = 0 \tag{10}$$

where the subscript *a* signifies dry air, *e* represents moist air, *d* represents liquid water forming the droplets. Enthalpies are shown as *h*, mass flow rates as $\dot{m}$, mass as *M*, and humidity ratio as ω.

Assuming constant specific heats, conservation of energy for a droplet can be written as

$$\dot{m}_{evap} h_{fg} + M_d C_{p,d} \frac{dT_d}{dt} = \alpha_{avg} \pi D_d^2 \left(T_e - T_d \right) \tag{11}$$

where h_{fg} is the heat of vaporization of water, and α_{avg} is the heat transfer coefficient calculated at the average of the droplet and the surrounding temperatures. α_{avg} is determined from the Nusselt number correlation developed by Faeth (1977) for Re<1800, evaluated at the average temperature.

The model was developed to handle a variety of operating conditions. Flow rates, initial droplet sizes, duct area, and Nusselt number correlation are among the parameters that can be easily adjusted.

3. WET CONDENSER MODEL

An analytical model for a condenser with a wetted surface was developed by applying the governing conservation and rate equations and invoking the heat and mass transfer analogy. The heat exchanger was discretized in both the air and refrigerant flow directions for a cross-flow configuration, as shown in Figure 2. Axial conduction along the tube walls was neglected and uniform distribution of water was assumed at the heat exchanger front fin surface. Any water not evaporated in a finite control volume was assumed to flow into the downstream control volume, and the model could handle, dry, partially wet, or fully wet surface conditions. Mass and energy balances are applied to each discretized volume (node) to examine the local heat and mass transfer.

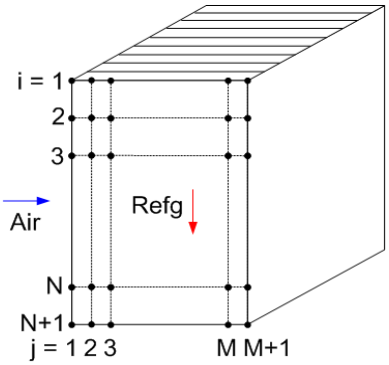

Figure 2: Discretization of heat exchanger

The model has the capability of predicting local heat/mass transfer, wetness condition as well as pressure losses throughout the heat exchanger. The veracity of the model was checked for two extreme cases: fully dry-surface conditions, and fully wet-surface conditions. The model converged to a dry condenser solution when very little water was applied. It converged to a fully wet condenser solution when water applied at the front surface was sufficient to reach fully wet conditions.

The governing equations were applied at each discretized node, which included the mass balance and energy balance equations. The built-in EES library of fluids was used to evaluate fluid properties.

3.1 Mass Balance

A water mass balance is given by Equation (12), where $\dot{m}_{evap}$ is the evaporation rate and $\dot{m}_{w}$ is the flow rate of water on the surface entering and exiting a given location, "*in*" and "*out*", respectively.

$$\dot{m}_{evap} = \dot{m}_{w,in} - \dot{m}_{w,out} \tag{12}$$

Using an air-side Nusselt number correlation from the literature to obtain Nu_{as}, and the heat and mass analogy, in the form of Equations 2-5, the mass transfer rate, or evaporation rate, is obtained by the maximum, or potential evaporation rate calculated by Equation (13), where A_{as} is the air-side heat transfer area in the node.

$$\dot{m}_{evap.\max} = g_m^* \beta_m A_{as} \tag{13}$$

However, the evaporation rate was constrained by the amount of available water; i.e, it is not possible to evaporate more than the water supplied to the node. As a result, the evaporation rate was determined by Equation (14). This approach ensured physically realistic evaporation rates for partially wet heat exchanger nodes.

$$\dot{m}_{evap} = \begin{cases} \dot{m}_{evap,\max} & \text{if } \dot{m}_{evap,\max} \le \dot{m}_{win} \\ \dot{m}_{water,in} & \text{if } \dot{m}_{evap,\max} > \dot{m}_{w,in} \end{cases} \tag{14}$$

A "wetness factor" was introduced to describe the local wetness condition of the heat exchanger surface. The wetness factor provides a means for obtaining physically meaningful values representing the degree of wetness for a node, Z, as defined in Equation (15).

$$Z = \frac{\dot{m}_{w,in}}{\dot{m}_{evap,\max}} \tag{15}$$

When the node was fully wet, the potential evaporation rate was less than the water supply rate, so the evaporation rate is equal to the water supply rate, resulting in $Z=1$. When the node was partially wet, the potential evaporation rate was greater than the water supply rate, $0<Z<1$. When the node was dry, no water on the node surface, and $Z=0$. The "wetness factor" shows how the water distribution changes progressively within the condenser as evaporation occurs, and it demarks where dry-out will occur. A diagram showing an example wetness distribution, where the blue signifies the presences of water, is shown in Figure 3.

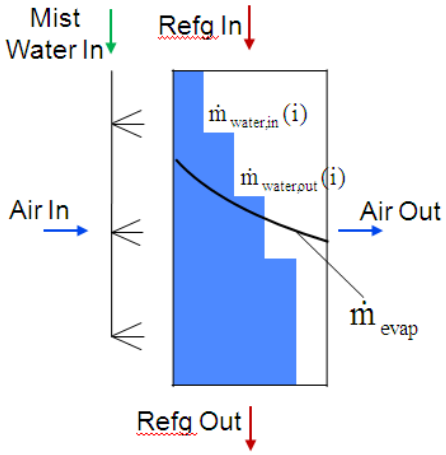

Figure 3: Water distribution in condenser

3.2 Energy Balance

The energy balance was written in various forms to evaluate multiple parameters. The rate at which heat is supplied to the moist air stream and due to the inflow and outflow of liquid water is described by the energy balance of Equation (16).

$$\dot{Q} = \dot{m}_{a,out} h_{a,out} - \dot{m}_{a,in} h_{a,in} - \dot{m}_{evap} h_{water} \tag{16}$$

The same rate of heat transfer must leave the tube-side flow; thus, using a rate equation with thermal resistances due to tube-side convection and wall conduction, and using an energy balance on the tube-side stream gives Equations (17) and (18).

$$\dot{Q} = \frac{T_{ts} - T_{w,s}}{R_{wall} + R_{ts}} \tag{17}$$

$$\dot{Q} = \dot{m}_{ts}\left(h_{ts,in} - h_{ts,out}\right) \tag{18}$$

The total capacity was divided to compare the latent and sensible contributions, as shown in Equation (19).

$$\dot{Q} = \dot{Q}_{sens} + \dot{Q}_{lat} \tag{19}$$

with

$$\dot{Q}_{lat} = \dot{m}_{evap} h_{fg} \tag{20}$$

$$\dot{Q}_{sens} = \frac{T_{w,s} - T_{as}}{R_{as}} \tag{21}$$

The thermal resistances are defined by Equations (22-24).

$$R_{wall} = \frac{l_t}{k_{Al} A_{bt}} \tag{22}$$

$$R_{as} = \frac{1}{\alpha_{as} A_{as}} \tag{23}$$

$$R_{ts} = \frac{1}{\alpha_{ts} A_{ts}} \tag{24}$$

Where the air-side heat transfer area, A_{as}, includes the fin efficiency for an adiabatic tip condition.

3.3 Heat Transfer Coefficients

The air-side and tube-side heat transfer coefficients, α_{as} and α_{ts}, respectively, were determined from existing correlations in the open literature. Appropriate air-side heat transfer coefficients were selected for the different heat exchanger configurations. For the louvered-fin microchannel heat exchanger used for model validation, the correlation proposed by Chang & Wang (1997) for the air-side heat transfer coefficient, α_{as}, was used. For the brazed flat-tube louvered fin heat exchanger used for model validation, the correlation developed by Park & Jacobi (2009) was used.

For subcooled refrigerant flow on the tube-side, the correlation by Churchill (1977) for round tubes was adopted, assuming a hydraulic diameter, and the friction factor was calculated using the Blasius (1913) correlation

$$f = 0.079\left(GD_h / \mu\right)^{-0.25} \tag{25}$$

For two-phase flow, the correlation developed by Shah (1979) for heat transfer coefficient at Re>350 was adopted.

3.4 Pressure Drop Correlations

The air-side and tube-side pressure drop correlations were determined from existing correlations in the open literature. For the microchannel heat exchanger used for model validation, the air-side pressure drop correlation developed by Kim and Bullard (2002) for louvered fin geometries was adopted. For the brazed flat-tube louvered fin heat exchanger used for validation, the air-side pressure drop correlation proposed by Park & Jacobi (2009) was used.

Determination of the tube-side pressure drop is dependent on the type of flow. The pressure drop is a function of the pressure gradient due to friction, $(dp/dz)_f$, and a pressure gradient component due to acceleration, $(dp/dz)_a$, as shown by Equation (26).

$$\left(\frac{dP}{dz}\right)_{ts} = \left(\frac{dP}{dz}\right)_f + \left(\frac{dP}{dz}\right)_a \tag{26}$$

For a single-phase working fluid there is no accelerational contribution, for a diabatic two-phase flow, the accelerational pressure gradient[14] is:

$$\left(\frac{dP}{dz}\right)_a = \frac{d}{dz}\left(\frac{G^2 x^2}{\rho_v \varphi} + \frac{G^2 \left(1-x\right)^2}{\rho_l \left(1-\varphi\right)}\right) \tag{27}$$

with the void fraction from Baroczy (1965).

$$\varphi = \left(1 + \left(\frac{1-x}{x}\right)^{0.74} \left(\rho_v / \rho_l\right)^{0.65} \left(\mu_l / \mu_v\right)^{0.13}\right)^{-1} \tag{28}$$

For subcooled refrigerant flow $(dp/dz)_f$, was calculated as shown in Equation (29).

$$\left(\frac{dP}{dz}\right)_f = \frac{fG^2}{2\rho D_h} \tag{29}$$

For wet-wall or two-phase refrigerant flow $(dp/dz)_f$, could be calculated using the correlation developed by Sun and Mishima (2008), for low-pressure refrigerants such as R245fa. An appropriate correlation for the working fluid should be adopted. The model has been written such that correlations can be easily replaced to reflect refrigerant choice.

For the tested heat exchangers, which had single-phase liquid flow in the tube, the equation set was simplified to reflect single-phase (subcooled) tube-side flow. For the micro-channel heat exchanger, the working fluid was water, and the properties were evaluated by EES internal library. For the brazed flat-tube louvered fin heat exchanger, the working fluid was a 56% ethylene glycol-water mixture, with properties described by Equations (30-33) (fits to manufacturer's data).

$$\rho_{ts} = -0.0024 \cdot T_{ts}^{\,2} - 0.3414 \cdot T_{ts} + 1083.7 \tag{30}$$

$$k_{ts} = -3 \cdot 10^{-6} \cdot T_{ts}^{\,2} + 0.0008 \cdot T_{ts} + 0.349 \tag{31}$$

$$\mu_{ts} \cdot 1000 = 0.0039 \cdot T_{ts}^{\,2} - 0.2925 \cdot T_{ts} + 8.2967 \tag{32}$$

$$C_{p,ts} = 0.0039 \cdot T_{ts} + 3.1855 \tag{33}$$

with the units T_{ts} =[°C], ρ_{ts} =[kg/m^3], k_{ts} =[W/m·K], μ_{ts} =[Pa·s], and $C_{p,ts}$ =[kJ/kg·K].

4. VALIDATION

Experimental validation of the precooling model was conducted by UTRC (Wu *et al*. 2011) in an open-loop wind tunnel with a full-cone, air-atomizing spray nozzle that produced water droplets with an initial diameter of 20 microns. Three temperature measurements were taken in the duct length between the spray nozzle and the face of the heat exchanger, and one temperature measurement was taken upstream of the spray nozzle. The model temperature predictions and the experimental data agreed with the experimental data provided by UTRC within 5%.

The heat exchanger model was validating using two sets of data. A rigorous set of data was obtained at UIUC as described in Zhang *et al.* (2012), using a brazed flat-tube louvered fin heat exchanger and an ethylene glycol solution as the working fluid. A more limited set of data was provided by UTRC for a micro-channel heat exchanger with water as the working fluid.

The combined precooling and deluge model was compared to experimental data gathered at UIUC, as well as the dry model. As a summary of the results, Figure 4 plots the predicted capacity for all conditions against the experimental data. The model predictions agree with the experimental results within 20%, with an average deviation of 8.3%. These results strongly support the use of the model for predicting condenser performance.

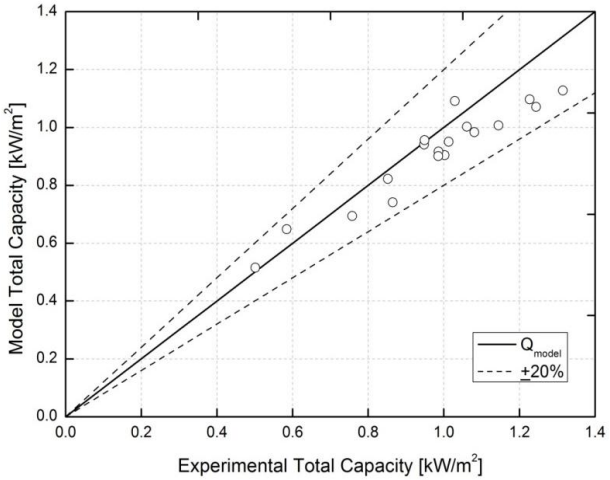

Figure 4: Comparison of UIUC experimental and predicted condenser performance for combined precooling and deluge cooling

The models were also validated with a limited set of experimental data provided by UTRC. The deviation of the experimental data from the predicted capacity is plotted in Figure 5 with lines indicating 20% deviation. The modeled capacity agrees with the measured capacity to within 20% for all of these experimental data.

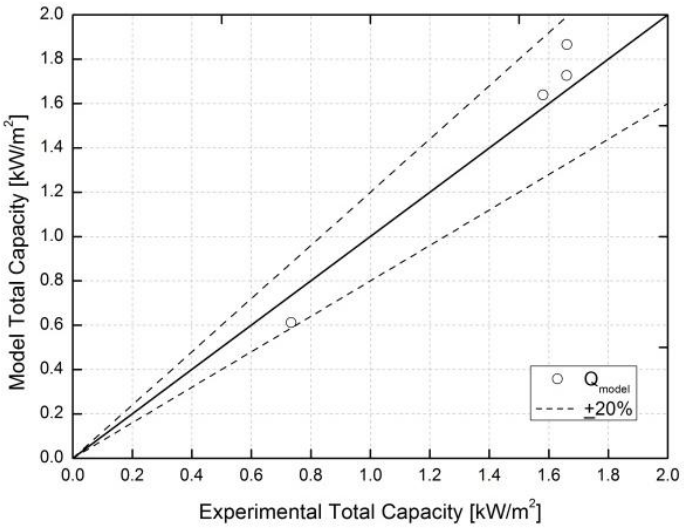

Figure 5: Comparison of UTRC experimental data and model predictions with lines showing 20% deviation

After validating the model, a range of conditions were explored in order to determine their effects on condenser performance. In many cases, minimizing the amount of required water may be a concern. With this in mind, the model was exercised to determine the effect of increasing water flow rates on condenser performance.

The model predicts an asymptotic behavior, such that at some point increasing the water flow rate no longer has an effect on the condenser performance, as seen in Figure 6, which was modeled using the operating conditions listed in Table 1. It also indicates that approximate 70% of the maximum capacity could be achieved by applying half of the water amount, 0.25 g/(m^{2}s). Similar asymptotic behavior was observed under various operating conditions for both brazed-fin and micro-channel heat exchangers, as well as single-phase and two-phase tube-side flow.

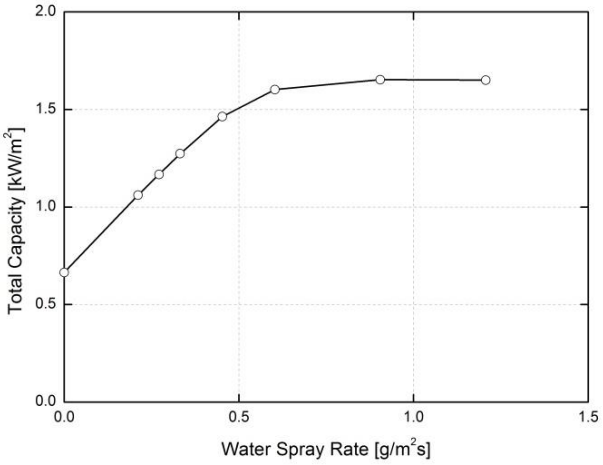

Figure 6: Heat capacity behaves asymptotically as the spray rate increases

Table 1: Operating conditions for Figure 7

T_{air}	23.9 °C
T_{water}	24 °C
RH	57.0 %
m_{air}	0.044 kg/m^{2}s
m_{refg}	0.033 kg/m^{2}s
T_{refg}	46.0 °C

5. CONCLUSION

An analytical model for a condenser with a wetted surface was developed by applying the governing conservation and rate equations and invoking the heat and mass transfer analogy. The heat exchanger was discretized in both the

air and refrigerant flow directions for a cross-flow configuration. Axial conduction along the tube walls was neglected and uniform distribution of water was assumed at the heat exchanger front fin surface. The physics-based model could handle dry, partially wet, or fully wet surface conditions. Mass and energy balances were applied to each discretized volume (node) to examine the local simultaneous heat and mass transfer. The model has the capability of predicting local heat/mass transfer, and wetness condition, as well as pressure losses throughout the heat exchanger. The model was developed to handle a variety of operating conditions, working fluids, and heat exchanger geometries and can be used in conjunction with an evaporative precooling model to evaluate different water augmentation configurations.

The model was validated with experimental data for a louver-fin microchannel heat exchanger with water on the tube-side, and a louver-fin brazed tube aluminum heat exchanger with an ethylene glycol solution on the tube-side. The total capacity, pressure drop, and water drainage behaviors under various water usage rates and air face velocities were explored for the brazed tube heat exchanger and compared with data for dry conditions. The data was obtained using an induced open-loop wind tunnel and a full cone water spray nozzle.

The results showed an increase in capacity and water drainage as the water supply rate increased. The total capacity exhibited asymptotic behavior, reaching a maximum value after which increasing the water supply rate no longer had an effect. As the water supply rate increases, drainage collection and recirculation systems should be considered.

NOMENCLATURE

A	area	(m^2)
α	heat transfer coefficient	($W/m^2 \cdot K$)
β	mass transfer driving force	(-)
Cp	specific heat	(kJ/kg·K)
D	diameter	(m)
$\mathcal{D}$	binary mass diffusivity	(m^2/s)
f	friction factor	(-)
G	refrigerant mass flux	($kg/m^2 \cdot s$)
g	mass conductance	($kg/m^2 \cdot s$)
g*	mass conductance at zero mass transfer	($kg/m^2 \cdot s$)
h	enthalpy	(kJ/kg)
k	thermal conductivity	(W/m·K)
l	thickness	(m)
M	mass	(kg)
$\dot{m}$	mass flow rate	(kg/s)
$\dot{m}''$	mass flux	($kg/m^2 \cdot s$)
μ	viscosity	(kg/m·s)
N	droplet production rate	(droplets/s)
Nu	Nusselt Number	(-)
ω	humidity ratio	(-)
P	pressure	(kPa)
φ	void fraction	(-)
Pr	Prandtl Number	(-)
Q	heat transfer	(W)
R	thermal resistance	(K/W)
ρ	density	(kg/m^3)
Sc	Schmitt Number	(-)
Sh	Sherwood Number	(-)
T	temperature	(°C)
t	time	(s)
x	quality	(-)
y	mass fraction	(-)

Subscripts

a	dry air
Al	aluminum
as	air-side
avg	average
bt	bare tube
evap	evaporative
D	diameter
d	droplet
e	moist air
fg	vaporization
h	hydraulic
i	initial
in	entering
l	saturated liquid
lat	latent
max	maximum
out	exiting
s	surface
sens	sensible
spray	water supply
t	tube
ts	tube-side
v	saturated vapor
w	water
wall	HX wall

Z	wetness factor	(-)
z	refrigerant flow length	(m)

REFERENCES

Ashwood, A., Bharathan, D., & National Renewable Energy Laboratory (U.S.), 2011. *Hybrid cooling systems for low-temperature geothermal power production*. National Renewable Energy Laboratory.

Baroczy, C. J., 1965. Correlation of liquid fraction in two-phase flow with applications to liquid metals. *Chem. Engr. Prog. Symp. Series*, vol. 61, no. 57, p. 179-191.

Blasius, H., 1913. Das Aehnlichkeitsgesetz bei Reibungsvorgängen in Flüssigkeiten. *VDI Mitt, Forschungsarb.* vol.131, p. 39.

Chang, Y. -J., & Wang, C. -C., 1997. A generalized heat transfer correlation for louver fin geometry. *International Journal of Heat and Mass Transfer*, vol. 40, no. 3, p. 533-544.

Churchill, S. W., 1977. Comprehensive correlating equations for heat, mass and momentum transfer in fully developed flow in smooth tubes. *Industrial and Engineering Chemistry Fundamentals*, vol. 16, no. 1, p. 109-116.

Faeth, G. M., 1977. Current status of droplet and liquid combustion. *Progress in Energy and Combustion Science*, vol. 3, no. 4, p. 191-224.

Fujita, A., Kurose, R., & Komori, S., 2010. Experimental study on effect of relative humidity on heat transfer of an evaporating water droplet in air flow. *International Journal of Multiphase Flow*, vol. 36, no. 3, p. 244-247.

Kim, M. -.H., & Bullard, C. W., 2002. Air-side thermal hydraulic performance of multi-louvered fin aluminum heat exchangers. *International Journal of Refrigeration*, vol. 25, no. 3, p. 390-400.

Kutscher, C, Costenaro, D., 2002, Assessment of evaporative cooling enhancement methods for air-cooled geothermal power plants, *Geothermal Resources Council Annual Meeting*, Reno, Nevada.

Mines, G., 2005, Evaluation of hybrid air-cooled flash/binary power cycle, *Geothermal Resources Council Annual Meeting*, Reno, Nevada.

Park, Y. -G., & Jacobi, A. M., 2009. The air-side thermal-hydraulic performance of flat-tube heat exchangers with louvered, wavy, and plain fins under dry and wet conditions. *Journal of Heat Transfer*, vol. 131, no. 6, p. 1-13.

Shah, M. M., 1979. A general correlation for heat transfer during film condensation inside pipes. *International Journal of Heat and Mass Transfer*, vol. 22, no. 4, p. 547-556.

Sun, L., & Mishima, K., 2009. Evaluation analysis of prediction methods for two-phase flow pressure drop in mini-channels. *International Journal of Multiphase Flow*, vol. 35, no. 1, p. 47-54.

Whitaker, S., 1972. Forced convection heat transfer correlations for flow in pipes, past flat plates, single cylinders, single spheres, and for flow in packed beds and tube bundles. AIChE Journal, vol. 18, no. 2, p. 361-371.

Wu, H. *et al.* 2011. Hybrid-cooled and enhanced turbine ORC; Internal Report. *UnitedTechnologies Corporation*. Hartford, Connecticut.

Zhang, F., Bock, J., Jacobi, A.M., & Wu, H., 2012, Simultaneous heat and mass transfer in a wetted heat exchanger, part I: experiments. *14th International Refrigeration and Air Conditioning Conference*. Paper #2239.

ACKNOWLEDGEMENT

This material is based upon work supported by the Department of Energy [Geothermal Technologies Program] under award DE-EE0002738 [Optimization of Hybrid-water/air-cooled Condenser in an Enhanced Turbine Geothermal ORC System] to the United Technologies Research Center (PI: Dr. Hailing Wu). This paper was prepared as an account of work sponsored by an agency of the United States Government. Neither the United States Government nor any agency thereof, nor any of their employees, makes any warranty, express or implied, or assumes any legal liability or responsibility for the accuracy, completeness, or usefulness of any information, apparatus, process, or process disclosed, or represents that its use would infringe privately owned rights. Reference herein to any specific commercial product, process, or service by trade name, trademark, manufacturer, or otherwise does not necessarily constitute or imply its endorsement, recommendation, or favoring by the United States Government or any agency thereof. The views and opinions of authors expressed herein do not necessarily reflect those of the United States Government or any agencies thereof. The authors are grateful for the support of the Department of Energy (DOE).